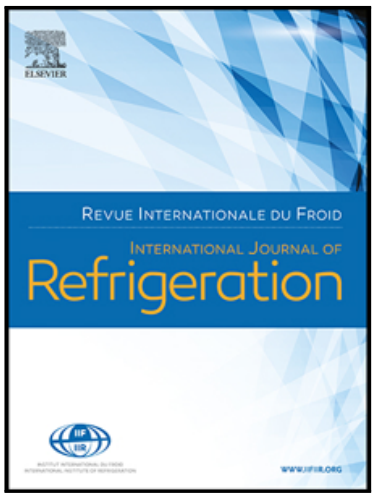

Thermodynamic and process modeling of the recovery of R410A compounds with ionic liquids

S. Asensio-Delgado , D. Jovell , G. Zarca , A. Urtiaga , F. Llovell

PII: S0140-7007(20)30160-2
DOI: https://doi.org/10.1016/j.ijrefrig.2020.04.013
Reference: JIJR 4743

To appear in: *International Journal of Refrigeration*

Received date: 20 December 2019
Revised date: 2 March 2020
Accepted date: 13 April 2020

Please cite this article as: S. Asensio-Delgado , D. Jovell , G. Zarca , A. Urtiaga , F. Llovell , Thermodynamic and process modeling of the recovery of R410A compounds with ionic liquids, *International Journal of Refrigeration* (2020), doi: https://doi.org/10.1016/j.ijrefrig.2020.04.013

Highlights

- A soft-SAFT model is used to describe the solubility of R410 compounds in ILs.
- Henry constants, the enthalpy and entropy of dissolution are predicted.
- $[C_2mim][Tf_2N]$ is chosen based on selectivity and solubility predictions.
- The ternary diagram IL-R32-R125 is built to evaluate the competitive selectivity.
- A process recovery simulation unit using $[C_2mim][Tf_2N]$ is optimized.

Thermodynamic and process modeling of the recovery of R410A compounds with ionic liquids

S. Asensio-Delgado[1], D. Jovell[2], G. Zarca[1], A. Urtiaga[1], F. Llovell[2*]

[1]*Department of Chemical and Biomolecular Engineering, Universidad de Cantabria, Av. Los Castros s/n, Santander 39005, Spain.*

[2]*Department of Chemical Engineering and Materials Science, IQS School of Engineering, Universitat Ramon Llull, Via Augusta 390, Barcelona 08017, Spain*

*Corresponding author: felix.llovell@iqs.edu Phone: +34 93 2670000

Abstract

European regulations are limiting the use of hydrofluorocarbons (HFCs) as refrigerants because of their elevated global warming potentials (GWPs). Apart from their substitution by other compounds with lower environmental impact, one of the plausible approaches to meet the legal requirements is the formulation of new refrigerant blends containing a low GWP compound (e.g. hydrofluoroolefins) mixed with one HFC that provides the necessary thermodynamic characteristics to act as an effective refrigerant. Thus, the recovery and reuse of HFCs seems a promising approach to increase their lifespan and reduce their production. However, current regeneration technologies that are based on distillation are highly energy-intensive. Therefore, the development of novel separation processes to selectively separate HFCs is needed for the practical implementation of circular economy principles in the use of refrigerants. This work is a step forward on using ionic liquids (ILs) to selectively separate F-gases. The advanced molecular-based soft-SAFT equation of state (EoS) is used as a tool to assess the potential of ILs as a solvent platform for the selective separation of the compounds forming the R410A refrigerant blend: R32 and R125. Soft-SAFT is employed to model the absorption of these HFCs into different ILs with different fluorinated anions. Ternary diagrams are then predicted for the absorption of R32/R125 mixtures into selected ILs to evaluate the competitive selectivity between both compounds. Based on this study, a

potential ionic liquid candidate is chosen and a process simulation is performed to estimate the approximate energy cost of the separation and recovery process.

Keywords: ionic liquid, R410A, soft-SAFT, solubility, selectivity, process simulation

Nomenclature

Abbreviations

AAD	Absolute Average Deviation
EOS(s)	Equation(s) of State
EU	European Union
GWP	Global Warming Potential
HFC	Hidrofluorocarbons
IG	Ideal Gas
IL(s)	Ionic Liquid(s)
LJ	Lennard-Jones
LLE	Liquid-Liquid Equilibria
LLV	Liquid-Liquid-Vapor
NIST	National Institute of Standards and Technology
NRTL	Non-Random Two-Liquid
SAFT	Statistical Association Fluid Theory
VLE	Vapor-Liquid Equilibria
VLLE	Vapor-Liquid-Liquid Equilibria
WEEE	Waste Electrical and Electronic Equipment

Latin symbols

A	Helmholtz free energy
f	Fugacity
g	Radial distribution function
k_B	Boltzmann constant
k_H	Henry's coefficients
K^{HB}	Volume of association
m	Chain length
M	Total number of association sites
P	Pressure
R	Ideal gas constant
S	Gaseous absorption selectivity
T	Temperature
V	Volume
x	Liquid mole fraction
X	Fraction of molecules not bonded to the site
y	Vapor mole fraction
z	Feed mole fraction

Greek symbols

α	Ideal selectivity
ε	Lennard-Jones energy parameter
ε^{HB}	Square-well energy parameter of an association site
η	Lorentz-Berthelot size binary parameter
ξ	Lorentz-Berthelot energy binary parameter
σ	Lennard-Jones size parameter (diameter of the sphere)

ρ	Density
ω	Acentric factor

Superscripts

assoc	Association
HB	Hydrogen bonding
id	Ideal
res	Residual
V	Vapor

Subscripts

α, β	Association sites
i, j	Compound

1. Introduction

Since the phase-out of ozone-depleting substances under the Montreal Protocol, the use of hydrofluorocarbons (HFCs) as alternative refrigerants with a negligible impact on the atmospheric ozone layer grew rapidly. Today, the concentration of HFCs in the atmosphere is still increasing due to fugitive emissions, the lack of end-life recovery protocols and the non-recyclability of refrigerants (Mota-Babiloni et al., 2017). However, the release of HFCs to the atmosphere is also a matter of concern because they are powerful greenhouse gases that, in some cases, exhibit very high Global Warming Potentials (GWPs). Therefore, international initiatives aiming at the reduction of HFCs emissions have been recently adopted. In this respect, EU Regulation No. 517/2014 (Schulz and Kourkoulas, 2014) established restrictions on the placing on the market of several products and equipment based on the intended application and the GWP of the HFC to be used. Moreover, the Kigali Amendment to Montreal Protocol, which schedules an ambitious program to reduce the production and consumption of HFCs (Heath, 2017), was ratified by numerous parties and entered into force on January 2019 intending to avoid up to 0.5 °C of warming by the end of the 21st century. Accordingly, some of the currently most employed HFC compounds in refrigeration and air conditioning, e.g., R134a (GWP = 1430), R404A (GWP = 3922) and R410A (GWP = 2088), must be replaced in the short-term by environment-friendly and energy-efficient alternative refrigerants (Mota-Babiloni et al., 2015).

One of the plausible approaches to meet both the legal and technical requirements is the formulation of new refrigerant mixtures, based on a low GWP compound (e.g. hydrofluoroolefins) combined with small amounts of at least one the following HFCs: difluoromethane (R32), pentafluoroethane (R125), 1,1,1,2-tetrafluoroethane (R134a) and 1,1-difluoroethane (R152a) (Mota-Babiloni et al., 2015). Moreover, EU Directive 2012/19 on waste electrical and electronic equipment (WEEE) (European Parliament and Council, 2012) compels the Member States to remove refrigerant fluids from separately collected WEEEs and ensure a proper treatment. Thus, this regulatory framework provides an excellent opportunity to shift towards a more circular economy as the waste refrigeration equipment that will be generated within the next decades will represent an important source of HFCs that could be reused (Pardo et al., 2020). Consequently, in order to boost the recyclability of refrigerants, the selective recovery of HFCs from end-of-life equipment and reuse in new refrigerant mixtures

must be sought. However, currently used HFC blends are characterized for behaving almost like pure fluids (near-azeotropic mixtures), with virtually no variation of composition between the vapor and liquid phases and almost constant evaporation/condensation temperature at a given pressure. Under these premises, the separation of the different HFCs by means of cryogenic distillation processes becomes really challenging (Ren and Scurto, 2009). Thus, it is necessary to develop new cost-effective processes to selectively separate refrigerant mixtures into their main constituents.

In this regard, ionic liquids (ILs) have been proposed for this purpose as a novel solvent platform in new gas separation processes because of their unique features, e.g., extremely low vapor pressure, high thermal and chemical stability, liquid state in a wide temperature range, and enhanced solvation properties, among others (Lei et al., 2014; Zarca et al., 2018; Zhao et al., 2017). Up to date, several studies have been conducted on the solubility of fluorinated refrigerants into ILs (Liu et al., 2015a, 2015b, 2015c, 2018; Shiflett and Yokozeki, 2006a, 2006b, 2006c, 2007, 2008; Yokozeki and Shiflett, 2006), concluding that the solubility is greater in ILs whose anion contains fluorinated groups (Dong et al., 2011; Shariati et al., 2005). While most studies primarily focused on assessing the phase equilibria of binary refrigerant/IL systems, Shiflett and Yokozeki initially proposed the separation of the R410A mixture using [C_4mim][PF_6] (Shiflett and Yokozeki, 2006d) and further described the utilization of ILs for separation, purification, and recycling of refrigerants and fluorinated monomers in several patents (Noelke and Shiflett, 2013; Shiflett et al., 2011; Shiflett, 2015; Shiflett and Yokozeki, 2014a, 2014b, 2012, 2011). Still with that, it is desirable to gain a deeper understanding of the feasibility of employing other fluorinated ILs to separate a refrigerant blend through evaluating the phase behavior of the ternary system formed by the IL and the HFCs mixture.

In literature, different theoretical approaches have been satisfactorily used to describe the phase behavior of IL/gas mixtures based on pure compound characteristics (Vega et al., 2010). Regarding IL/F-refrigerants, Shiflett and coworkers were the first to measure and model these mixtures in a series of papers published since 2006 using activity coefficient methods, namely, the Non-Random Two Liquid (NRTL) model (Shiflett et al., 2006a; Shiflett and Yokozeki, 2008, 2006e, 2006c) and the Redlich-Kwong (RK) cubic EoS (Shiflett and Yokozeki, 2006b). Its pioneering contributions included the

description of VLE and also the VLLE line for systems involving common refrigerants in ILs with different anions, obtaining very good agreement when comparing to experimental data. The reader is referred to the review chapter published by these authors, where a summary of their work can be found (Shiflett and Yokozeki, 2009). Later, Kim and coworkers also used NRTL (Kim et al., 2012) and RK (Kim et al., 2013; Kim and Kohl, 2014) to thermodynamically evaluate the efficiency of the refrigerant- IL absorbent pairs. More recently, molecular-based methods such as the Statistical Associating Fluid Theory (SAFT) have also been used to assess these mixtures (Sujatha and Venkatarathnam, 2018).

The aim of this work is to assess the feasibility of the selective recovery of HFCs from common refrigerant mixtures contained in waste refrigeration equipment using ILs. In doing so, the recovered HFCs could be further reused to produce new HFC refrigerant mixtures, thus increasing their lifetime and minimizing the amount of new fluorinated gases placed into the market. We focus our attention on evaluating the technical viability of splitting into its individual components the refrigerant blend R410A that is going to be phased out in air conditioning applications. Refrigerant R410A is a near-azeotropic mixture formed by R32 and R125, whose main characteristics are summarized in **Table 1**. To that end, the phase behavior of the refrigerant gases R32 and R125 as well as that of their mixtures will be described using the soft-SAFT EoS (Blas and Vega, 1998, 1997). Next, the solubility of these gases into different ILs will be evaluated with the same equation. Three fluorinated ILs are considered based on their potential use in novel separations and the availability of experimental HFCs solubility data: 1-butyl-3-methylimidazolium hexafluorophosphate ([C_4mim][PF_6]), 1-hexyl-3-methylimidazolium bis(trifluoromethylsulfonyl)imide ([C_6mim][Tf_2N]), and 1-ethyl-3-methylimidazolium bis(trifluoromethylsulfonyl)imide ([C_2mim][Tf_2N]). The possible interactions between the refrigerant gases and these ILs will be ascertained by predicting the high-pressure phase behavior of the ternary mixtures formed by the two HFCs and each IL, as well as the expected separation performance of the gas-liquid separation. Based on this study, a potential IL candidate is selected and a process simulation of the recovery unit is performed to estimate the approximate energy cost of the separation process.

2. Theory

2.1. soft-SAFT

The soft-SAFT EoS (Blas and Vega, 1997) is a successful variant of the original SAFT EoS (Chapman et al., 1990, 1989), which modifies the reference term of the original SAFT theory by a Lennard-Jones (LJ) dispersion term. The equation has already been proved to accurately reproduce the thermophysical properties of fluorinated refrigerants, such as hydrofluorocarbons (Llovell et al., 2013; Vilaseca et al., 2010) and hydrofluoroolefins (Albà et al., 2020), as well as the solubility of other greenhouse gases (CO_2, SO_2, N_2O, CO) in many ILs (Andreu and Vega, 2008, 2007; Llovell et al., 2015; Oliveira et al., 2012; Pereira et al., 2016, 2014, 2013; Zarca et al., 2017a, 2017b).

Soft-SAFT is written in terms of the different microscopic contributions to the residual molar Helmholtz free energy

$$A^{res} = A - A^{id} = A^{ref} + A^{chain} + A^{assoc} \quad (1)$$

where the subscripts *id*, *ref*, *chain* and *assoc* refer to the ideal, reference, chain and association terms, respectively. These terms include a total of five molecular parameters defining the fluid: the chain length (m), the characteristic segment diameter (σ_{ii}), the dispersive energy) (ε_{ii}/k_B) and the volume ($K^{HB}_{\alpha\beta,ii}$) and energy ($\varepsilon^{HB}_{\alpha\beta,ii}$) of association. For mixtures, the Lorentz-Berthelot combining rules are applied and two binary parameters, η_{ij} and ξ_{ij}, account for deviations in the crossed segment diameter and dispersive energy of the mixtures. Further details of the different terms of soft-SAFT are provided in the Supplementary Information (section A), while for a whole analysis of the equation the reader is referred to the original soft-SAFT contributions *(Blas and Vega, 1998, 1997).*

2.2. Molecular models

HFCs are considered homonuclear chainlike molecules modeled as several segments (m) of equal diameter (σ) and dispersive energy (ε/k_B). The strong dipole moments due to the electronegativity of fluorine atoms (Costa Cabral et al., 2001) are considered through the association term by incorporating two associating sites of different nature (type A and B) and equal association energy (ε^{HB}/k_B) and volume (K^{HB}). Both self-association (A-B interactions) between molecules of the same refrigerant and, for binary HFCs mixtures, cross-association (A-B' and A'-B interactions) between different refrigerant molecules are allowed.

Regarding ILs, molecular dynamics simulations have evidenced that this type of Coulombic fluids form ionic clusters in which cations and anions are coupled together

(Del Pópolo and Voth, 2004; Urahata and Ribeiro, 2004). For this reason, ILs are typically modeled as Lennard-Jones chains with specific association sites describing the interactions between ions that derive from their ionic nature and the asymmetric charge distribution of molecular ions. In particular, the $[C_x mim][PF_6]$ ILs have been modeled with a single associating site (type C) mimicking the strong cation-anion interactions (Andreu and Vega, 2007; Llovell et al., 2012). On the other hand, the model proposed for the $[C_x mim][Tf_2N]$ ILs considers three association sites: one site (type D) represents the nitrogen atom interactions with the cation, and two sites (type E) take into account the delocalization of the anion electric charge due to the presence of the oxygen groups (Llovell et al., 2011). Both self-association interactions (C-C and D-E) between different molecules of the same IL and cross-association interactions with the refrigerant molecules (A-C, B-C, A-D and B-E) are considered to model the phase behavior of HFC + IL systems in this work.

The molecular parameters of HFCs and ILs used in this study are collected in **Table 2**. The optimized parameters of ILs were obtained from the abovementioned works (Andreu and Vega, 2007; Llovell et al., 2011), while the parameters for R32 and R125 have been reparametrized here. The main reason is that the original contribution (Vilaseca et al., 2010) included a renormalization group treatment for the critical region (Llovell et al., 2004), not used here. This slightly worsened the description of the vapor pressure with the previous parameters, which were here refined by refitting the dispersive energy, as done for R125. Concerning R32, the original restriction forcing this molecule to be modeled as a sphere (so m=1) was removed, based on the fact that the non-sphericity of this compound is evident from observation of its chemical structure geometry and acentric factor value (ω=0.2769). The new R32 parametrization provides a better overall description of the molecule in a wide range of temperatures, as it will be shown in the next section.

3. Results and discussion

3.1. Phase behavior of HFCs

The phase envelope of both refrigerants calculated with the new molecular parameters is depicted in **Figure 1**, where the temperature-density (**Figure 1a**) and the pressure-temperature (**Figure 1b**) diagrams are described with soft-SAFT and compared to NIST correlated data (Linstrom and Mallard, 2014). An excellent

description is found in a wide range of temperatures, from close to the triple point up to 95% of the critical point. The critical point is slightly overestimated due to the absence of the crossover treatment and this produces a slight underestimation of the vapor pressure of R32 at the highest temperatures. Nevertheless, the relative average deviation (AAD%) respect to the experimental data is very low for both the saturated liquid density calculations (AAD%) (1.13% and 0.21% for R125 and R32, respectively) and the vapor pressure (3.48% and 1.52% for R125 and R32, respectively).

The molecular models proposed for R32 and R125 are then used to calculate the phase behavior of their mixtures. The binary mixture R32 + R125 is a near-azeotropic blend that forms a slightly positive pressure azeotrope at a composition of 91 mol % R32 (Higashi, 1997). The soft-SAFT description of the vapor-liquid equilibria (VLE) of this system at temperatures ranging between 283.15 and 323.15K is given in **Figure 2**, where the model is compared to the available experimental data (Higashi, 1997). A temperature-independent energy binary parameter has been fitted to an intermediate isotherm at 303.15 K and transferred to predict the VLE of this system at the other temperatures. An accurate description of the phase equilibria is obtained in the whole composition range using a value of ξ=0.955. Minor deviations are found at the highest temperature (T=323.15 K) because of the underprediction of the pure vapor pressures, affecting the performance of the binary model.

Once the interactions between R32 and R125 have been adequately characterized, the VLE of the refrigerant blend R410A is predicted with soft-SAFT by transferring the binary parameter previously fitted. The temperature-density and pressure-temperature diagrams of R410A, plotted in **Figures 3a** and **3b**, respectively, reveal an excellent agreement between the experimental (correlated) data (Honeywell Genetron Properties Suite, 2016) and the predicted values.

3.2. Binary mixtures of HFCs and ILs

The following step consists in modeling the behavior of R32 and R125 in the presence of ILs. **Figure 4** and **Figure 5** show the solubility of both refrigerants in $[C_2mim][Tf_2N]$ and $[C_4mim][PF_6]$, respectively. Results with $[C_6mim][Tf_2N]$ are also provided as **Supplementary Information**, in **Figure S1**. In all cases, the size and energy binary parameters were fitted to one isotherm (298.15 K) and used to predict the rest of them. The list of the optimized binary parameters is collected in **Table 3**.

The optimized binary parameters have similar values, regardless of the IL. In particular, the size binary parameter, η, is constant for all cases except for the R125 + [C_4mim][PF_6], whose value is slightly higher in order to capture the convex nature of the solubility curve at low temperatures. This means that the influence of the IL in the volume interactions (entropic effects) is almost negligible, allowing predictions of the solubility of these compounds in other ILs. The energy binary parameter, ξ, has similar values for the two [Tf_2N]-based ILs, indicating that the effect of the alkyl chain in the cation is minor in the description of the association interactions. This information is useful to check the transferability of these parameters to other compounds when no experimental data are available. A final comment concerns the value of the ξ parameter which, in all cases, is remarkably higher than one, meaning the classical Lorentz-Berthelot combining rules underestimate the solubility of the refrigerant in the IL. This might be an indication that the model for the mixture is missing some interactions. Also, the size binary parameter is higher than one, increasing the miscibility of the refrigerant at high mole fractions.

Overall, the description of the solubility of these systems is very good at all temperatures, agreeing with the available experimental data (Shiflett et al., 2006b; Shiflett and Yokozeki, 2008; Yokozeki and Shiflett, 2006). Moreover, the soft-SAFT model predicts an immiscibility gap at very high concentrations of R32 and R125 for all ILs. The R125 gap is more significant and occurs around 80% of R125. The presence of an immiscible region was also found by Shiflett and Yokozeki (Shiflett and Yokozeki, 2008) in the mixture R125 + [C_2mim][Tf_2N]. These authors measured some VLLE data, which is used here for comparison. Our predicted VLLE is in good agreement with the previous data, although it is slightly larger. On the other hand, the same authors (Shiflett et al., 2006b) did not find any immiscibility gap for the mixtures with R32 + [C_2mim][Tf_2N], when they modeled their data using the nonrandom two-liquid (NRTL) activity coefficient model.

From the results discussed above, Henry's coefficients (k_H), which relate the amount of gas dissolved in the liquid (x) to the vapor phase fugacity of the solute in equilibrium with the solvent (f^V) at infinite dilution and constant temperature, are calculated from the slope of the absorption isotherm at very low pressures.

$$k_H(T) = \lim_{x\to 0} \frac{f^V(P,T)}{x} \qquad (2)$$

The temperature influence on the Henry's law constants is described following the expression (Liu et al., 2015a):

$$\ln k_H = \frac{A}{T} + B \quad (3)$$

where A and B are the experimental regression coefficients provided in **Table S1** of the **Supplementary Information**.

Figure 6 plots the calculated Henry's law constant of R32 and R125 in the ILs under study. As can be seen, the solubility of R32 is higher than that of R125 in all cases. Also, the ILs with the [Tf_2N] anion exhibit slightly higher sorption capacities than [C_4mim][PF_6], as they have lower Henry's constants. In addition, the influence of temperature on the Henry's constants is very similar for R32 and R125 in each IL, as deducted from **Table S1**.

The theoretical performance of these ILs to separate R410A compounds is firstly approached by defining the ideal selectivity, α, calculated at infinite dilution as:

$$\alpha_{R32/R125} = \frac{k_H^{R125}}{k_H^{R32}} \quad (4)$$

The selectivity values, also plotted in **Figure 6** for each IL, follow the opposite trend to that observed in gas solubility, as the ideal selectivity is higher for [C_4mim][PF_6] than for the [Tf_2N]-based ILs. This is a consequence of the lower solubility of R125 at low compositions of [C_4mim][PF_6]. This difference decreases at higher pressures, as it is shown by additionally plotting the ideal selectivity at 1.0 MPa, calculated from the VLE modeled data (**Figures 4, 5 and S1**). At this pressure, which is likely to be employed in an extractive distillation process in order to increase gas sorption throughout and reduce the amount of IL to be used, all three ILs provide similar selectivity values. Consequently, selecting the best IL to perform the separation becomes difficult if the comparison is made only in terms of absorption capacity and selectivity, as there are no significant differences among them. Mass transfer is another key factor affecting the performance of gas separation processes (Mota-Martinez et al., 2018). Using [C_2mim][Tf_2N] would favor the separation because its viscosity (34 mPa s at 298 K) is twofold and tenfold lower than [C_6mim][Tf_2N] (71 mPa s at 298 K) and [C_4mim][PF_6] (329 mPa s at 298 K), respectively (Ahosseini and Scurto, 2008; Harris et al., 2005). Moreover, [PF_6] anion is less stable as it can hydrolyze in the presence of water (Wasserscheid et al., 2002). Therefore, [C_2mim][Tf_2N] is selected in this work to further assess the separation of R32 from R125 using ILs.

Finally, the van't Hoff equation is used to obtain the enthalpy (Eq. (5) and entropy (Eq. (6)) of dissolution of the mixtures (Blath et al., 2011) using the data obtained from soft-SAFT to evaluate the dependence of the solvation process on temperature.

$$\Delta H_{dis} = R\left(\frac{\partial \ln k_H}{\partial (1/T)}\right)_p \quad (5)$$

$$\Delta S_{dis} = -R\left(\frac{\partial \ln k_H}{\partial \ln T}\right)_p \quad (6)$$

The results of the calculation of solvation enthalpies and entropies are presented in **Table 4.** The magnitude of the solvation enthalpies of R32 and R125 are within the typical range of physical sorption and are just slightly higher than that found for CO_2 sorption in these ILs (Cadena et al., 2004).

3.3. *Phase behavior of ternary mixtures*

The information gathered from the study of the binary systems is used to predict, in the absence of experimental data, the phase behavior of ternary mixtures formed by the two HFCs and the candidate IL, [C_2mim][Tf_2N], selected to perform the separation. The ternary diagram R32 + R125 + [C_2mim][Tf_2N] at 300 K is presented in **Figure 7.** Several isobars were calculated to assess the influence of pressure on the phase behavior of the mixture, and the corresponding liquid composition is indicated in the diagram. A region of immiscibility, i.e., liquid-liquid equilibrium (LLE), is found at high compositions of both refrigerants above 1.4 MPa, as expected from the information gathered in the binary systems. The three VLLE phase line has been estimated and indicated in the diagram as a dashed line. Similar diagrams have been reported for the absorption into ILs of very soluble gases such as CO_2 and SO_2 (Shiflett and Yokozeki, 2010; Yokozeki and Shiflett, 2009).

Using the ternary diagrams, the performance of the gas separation for a given inlet composition is reevaluated by defining the gaseous absorption selectivity, S, as follows (Yokozeki and Shiflett, 2007):

$$S_{R32/R125} = \frac{y_{R125}/x_{R125}}{y_{R32}/x_{R32}} \quad (7)$$

where x and y denote the molar composition of R32 and R125 in the solvent liquid and vapor phases, respectively. This is a more realistic value than that obtained from Eq. (4), as it includes the competition between the two HFCs. In Eq. (7), the vapor compositions in equilibrium with the liquid are calculated as a function of the IL concentration in the feed (z_{IL}) and the operating pressure through an iterative process that involves solving

the Rachford-Rice flash equation. The separation performance for the mixture R410A provided by [C_2mim][Tf_2N] at 300 K is presented in **Figure 8**. The predicted value of separation performance tends to the calculated ideal selectivity at infinite dilution and decreases, as expected, with pressure. Moreover, although lower pressures yield higher separation performances (closer to the ideal selectivity), this occurs at the expense of lower sorption capacity and consequently, lower recovery. At higher pressures, the predicted LLE immiscibility region also limits the amount of gas that can be recovered. Nevertheless, very high-pressure operating conditions do not seem to be attractive because they incur in ~25% separation performance drops for a given IL feed composition.

4. Process Simulation

4.1. Configuration and implementation details

The thermodynamic characterization has been accompanied by a process simulation of the mixture separation of R32 and R125 at the proportions forming the R410A blend. The simulation is done through the design of an extractive distillation unit where the IL selected in the previous section, [C_2mim][Tf_2N], is used as entrainer. All simulations have been carried out with the Aspen Plus® v10 (36.0.0.249) simulator.

While the HFCs conforming R410 can be taken as conventional components from the Aspen Plus Database, the thermophysical properties of [C_2mim][Tf_2N] are required to be introduced in the system as no information was available in the ASPEN databank. The critical properties of the IL were taken from the literature. (Shariati et al., 2013). The ideal heat gas capacity was estimated using the extended Joback method (Ge et al., 2008). The vapor pressure information was taken from the data presented by Heym et al. (Heym et al., 2015). The Clausius-Clapeyron equation was applied to predict the heat of vaporization with liquid vapor pressure data since the vapor phase is assumed as an ideal gas and the molar volume of the liquid is negligible compared to that of the vapor. Finally, liquid viscosity data was obtained from the literature (Noda et al., 2001) and fitted to an Andrade-type equation, as the two-constant Arrhenius equation, suggested in by some authors (De Riva et al., 2014), was producing higher deviations. Further details on the numerical implementation of these properties into Aspen Plus, as well as the critical values, normal boiling point, acentric factor (ω) and all the optimized

constants for the ideal heat capacity, vapor pressure, enthalpy of vaporization and liquid viscosity correlations can be found in the **Supplementary Information, Section C.**

An extended version of the NRTL model is used to describe the nonideal behavior in the liquid phase of the mixture (see the **Supplementary Information** for further details), as done by many researchers to model the behavior of mixtures containing ILs (Meindersma et al., 2006; M. B. Shiflett et al., 2011; Vatani et al., 2012), while an ideal gas model (IG) is kept for the gas phase. The extended NRTL parameters are fitted to experimental data (Higashi, 1997; Shiflett et al., 2006b; Shiflett and Yokozeki, 2008) by minimizing a least-squares function including the calculated activity coefficients. The parameters obtained from the minimization are presented in **Table S4.**

Following the work of Shiflett and Yokozeki (Shiflett and Yokozeki, 2014b, 2006d), the process consisted of a main distillation column for the separation of R32 and R125 followed by two flash tanks for the regeneration of [C_2mim][Tf_2N] and an IL recirculation including a pump with a heat exchanger to cool the IL before returning to the main column (see **Figure 9)**.

The inlet flow of R410A introduced to the process was fixed to 0.3 kg s^{-1} and is considered an equimassic mixture of R125 and R32. Several configurations were tested to select the most appropriate column configuration to reach a purity of 99% mole.

Several pre-calculations have shown that a column with 28 stages, including the reboiler and the partial condenser, is necessary to reach the purity requirements for R125. This column operates at 1 MPa as in the publication of Shiflett and Yokozeki (Shiflett and Yokozeki, 2006d). The column has been modeled with the ASPEN RadFrac® module to account for the VLLE. Due to the non-ideal nature of the mixture, the column must be converged in two phases. In a first iteration, the highly non-ideal convergence method was selected and the key components of the three-phase equilibrium were established. To make the column numerically more robust, a second iteration comprises a custom convergence method that uses the Newton-Raphson algorithm. A maximum of 200 iterations have been considered along with Powell's algorithm to find local minimums of functions. The IL and the refrigerant mixture have been fed through stages 2 and 22, respectively, with a molar reflux ratio of 1.5 and a [C_2mim][Tf_2N] flow rate of 4.24 kg s^{-1} in order to meet the specified separation requirement.

The flash drums have been modeled with ASPEN two-outlet flash module, and the operating temperature has been set equal to the reboiler temperature (353.73 K). The fluid is depressurized when passing through a throttling valve so that part of the fluid can be vaporized for further separation. No IL is vaporized and gaseous R32 is obtained through the flash drums heads. Both drums are connected in series and operated adiabatically. The pressure drop is set at 0 MPa, being the operating pressure the same as that obtained after the valve expansion i.e. 0.1 MPa and 0.01 MPa respectively.

Due to the pressure changes that the IL undergoes during the separation process and the temperature changes that this entails, the solvent must be pressurized again, and its temperature must be lowered to the feed temperature. For this purpose, a pump and heat exchanger are provided to recirculate the entire solvent used in the separation.

4.2. Analysis of the results

Table 5 shows the ASPEN Plus simulation results for the separation of R410A using [C_2mim][Tf_2N] as entrainer. A distillate flow rate of 0.1218 kg s^{-1} with a mole fraction of R125 = 0.99 is obtained. This represents a 99.56w% with respect to the initial feed of R125. R32 is absorbed in the IL and later separated in the cascade system of flash separators, due to the pressure drop experienced by the mixture, obtaining a molar composition of 0.92 and 0.96 in the first and second flash separators, respectively. The IL is then recirculated to the column with minimal traces of R32 and R125.

The effect of the feeding stage of the HFC mixture on the purity of the distillate obtained in the first separation stage has been analyzed in order to select the most adequate configuration to perform the extractive distillation of [C_2mim][Tf_2N] + R410A. While the IL must be introduced in the early stages of separation to ensure as much contact as possible between the extracting agent and the mixture, this is not the case for the feeding stage of the R410A blend.

Several simulations were carried out to find the most suitable combination of the solvent and feed stage location that will maximize the purity of R32 and R125. As can be seen from **Figure 10**, the optimum feed location was estimated to be at stage 22.

5. Conclusions

In this work, the absorption and separation of R32 and R125, the two hydrofluorocarbons forming the R410A blend, using Ionic Liquids (ILs) has been theoretically addressed by means of the soft-SAFT molecular-based equation of state.

For that purpose, three imidazolium ILs containing two fluorinated anions, [PF_6] and [Tf_2N], have been selected and their capacity to absorb and selectively separate these HFCs has been evaluated. Using relatively simple coarse-grained molecular models for the HFCs and assuming a cation-anion pair with the charges represented by a certain number of associating sites, the solubility of R32 and R125 in the studied ILs has been characterized with soft-SAFT using two binary temperature-independent parameters. An excellent representation of the solubility curves is achieved at all compositions and temperature conditions. The immiscibility regions at high refrigerant compositions have been theoretically predicted. Also, the enthalpy and entropy of solvation, the Henry constants and the selectivity of these mixtures are evaluated and compared. Although results do not reveal significant differences from a thermodynamics perspective, [C_2mim][Tf_2N] is selected as the most promising solvent considering mass transfer and viscosity aspects. A ternary mixture is then predicted so as to build the thermodynamic diagram and evaluate the competitive selectivity. The results reveal low selectivity values in a range of values between 1 and 2 at 300 K. Even if the selectivity values are relatively low, a process simulation of the whole recovery process has been performed in order to study the feasibility of the separation. The thermodynamic properties of the IL have been fitted to available experimental data and introduced into the process simulators. The results reveal that it is possible to obtain a high yield of separation (99.56% of the initial mass) using a column of 28 stages and a reasonable amount of energy. While the focus of this work is on the use of molecular modeling tools to provide thermophysical information on the separation process, the simulations allow a predesign of a future unit equipment.

Acknowledgments

This research is supported by Project KET4F-Gas – SOE2/P1/P0823, which is co-financed by the European Regional Development Fund within the framework of the Interreg SUDOE Program. Also, S. Asensio-Delgado would like to thank the FPU grant (18/03939) awarded by the Spanish Ministry of Education.

References

Ahosseini, A., Scurto, A.M., 2008. Viscosity of imidazolium-based ionic liquids at elevated pressures: Cation and anion effects. Int. J. Thermophys. 29, 1222–1243.

https://doi.org/10.1007/s10765-008-0497-7

Albà, C.G., Vega, L.F., Llovell, F., 2020. A consistent thermodynamic molecular model of n-hydrofluorolefins and blends for refrigeration applications. Int. J. Refrig. 113, 145–155. https://doi.org/10.1016/j.ijrefrig.2020.01.008

Andreu, J.S., Vega, L.F., 2008. Modeling the solubility behavior of CO2, H2, and Xe in [Cn-mim] [Tf2N] ionic liquids. J. Phys. Chem. B 112, 15398–15406. https://doi.org/10.1021/jp807484g

Andreu, J.S., Vega, L.F., 2007. Capturing the solubility behavior of CO_2 in ionic liquids by a simple model. J. Phys. Chem. C 111, 16028–16034. https://doi.org/10.1021/jp074353x

Blas, F.J., Vega, L.F., 1998. Prediction of Binary and Ternary Diagrams Using the Statistical Associating Fluid Theory (SAFT) Equation of State. Ind. Eng. Chem. Res. 37, 660–674. https://doi.org/10.1021/ie970449+

Blas, F.J., Vega, L.F., 1997. Thermodynamic behaviour of homonuclear and heteronuclear Lennard-Jones chains with association sites from simulation and theory. Mol. Phys. 92, 135–150. https://doi.org/10.1080/002689797170707

Blath, J., Christ, M., Deubler, N., Hirth, T., Schiestel, T., 2011. Gas solubilities in room temperature ionic liquids - Correlation between RTiL-molar mass and Henry's law constant. Chem. Eng. J. 172, 167–176. https://doi.org/10.1016/j.cej.2011.05.084

Cadena, C., Anthony, J.L., Shah, J.K., Morrow, T.I., Brennecke, J.F., Maginn, E.J., 2004. Why is CO2 so Soluble in Imidazolium-Based Ionic Liquids? J. Am. Chem. Soc. 126, 5300–5308. https://doi.org/10.1021/ja039615x

Chapman, W.G., Gubbins, K.E., Jackson, G., Radosz, M., 1990. New reference equation of state for associating liquids. Ind. Eng. Chem. Res. 29, 1709–1721. https://doi.org/10.1021/ie00104a021

Chapman, W.G., Gubbins, K.E., Jackson, G., Radosz, M., 1989. SAFT: Equation-of-state solution model for associating fluids. Fluid Phase Equilib. 52, 31–38. https://doi.org/10.1016/0378-3812(89)80308-5

Costa Cabral, B.J., Guedes, R.C., Pai-Panandiker, R.S., Nieto de Castro, C.A., 2001. Hydrogen bonding and the dipole moment of hydrofluorocarbons by density

functional theory. Phys. Chem. Chem. Phys. 3, 4200–4207. https://doi.org/10.1039/b102879k

De Riva, J., Ferro, V.R., Del Olmo, L., Ruiz, E., Lopez, R., Palomar, J., 2014. Statistical refinement and fitting of experimental viscosity-to-temperature data in ionic liquids. Ind. Eng. Chem. Res. 53, 10475–10484. https://doi.org/10.1021/ie5014426

Del Pópolo, M.G., Voth, G.A., 2004. On the structure and dynamics of ionic liquids. J. Phys. Chem. B 108, 1744–1752.

Dong, L., Zheng, D., Sun, G., Wu, X., 2011. Vapor-liquid equilibrium measurements of difluoromethane + [Emim]OTf, difluoromethane + [Bmim]OTf, difluoroethane + [Emim]OTf, and difluoroethane + [Bmim]OTf systems. J. Chem. Eng. Data 56, 3663–3668. https://doi.org/10.1021/je2005566

European Parliament and Council, 2012. Directive 2012/19/EU of the European Parliament and of the Council of 4 July 2012 on waste electrical and electronic equipment (WEEE). Off. J. Eur. Union L197, 38–71.

Ge, R., Hardacre, C., Jacquemin, J., Nancarrow, P., Rooney, D.W., 2008. Heat capacities of ionic liquids as a function of temperature at 0.1 MPa. Measurement and prediction. J. Chem. Eng. Data 53, 2148–2153. https://doi.org/10.1021/je800335v

Harris, K.R., Woolf, L.A., Kanakubo, M., 2005. Temperature and pressure dependence of the viscosity of the ionic liquid 1-butyl-3-methylimidazolium hexafluorophosphate. J. Chem. Eng. Data. https://doi.org/10.1021/je050147b

Heath, E.A., 2017. Amendment to the Montreal Protocol on Substances that Deplete the Ozone Layer (Kigali Amendment). Int. Leg. Mater. 56, 193–205. https://doi.org/10.1017/ilm.2016.2

Heym, F., Korth, W., Thiessen, J., Kern, C., Jess, A., 2015. Evaporation and decomposition behavior of pure and supported ionic liquids under thermal stress. Chemie-Ingenieur-Technik 87, 791–802. https://doi.org/10.1002/cite.201400139

Higashi, Y., 1997. Vapor-liquid equilibrium, coexistence curve, and critical locus for difluoromethane + pentafluoroethane (R-32 + R-125). J. Chem. Eng. Data 42, 1269–1273. https://doi.org/10.1021/je9701083

Honeywell Genetron Properties Suite, 2016. European Refrigerants.

https://www.honeywell-refrigerants.com/europe/genetron-properties-suite.

IPCC — Intergovernmental Panel on Climate Change, 2015. Global Warming Potential Values. Greenh. Gas Protoc.

Kim, S., Kohl, P.A., 2014. Analysis of [hmim][PF6] and [hmim][Tf2N] ionic liquids as absorbents for an absorption refrigeration system. Int. J. Refrig. 48, 105–113. https://doi.org/10.1016/j.ijrefrig.2014.09.003

Kim, S., Patel, N., Kohl, P.A., 2013. Performance simulation of ionic liquid and hydrofluorocarbon working fluids for an absorption refrigeration system. Ind. Eng. Chem. Res. 52, 6329–6335. https://doi.org/10.1021/ie400261g

Kim, Y.J., Kim, S., Joshi, Y.K., Fedorov, A.G., Kohl, P.A., 2012. Thermodynamic analysis of an absorption refrigeration system with ionic-liquid/refrigerant mixture as a working fluid. Energy 44, 1005–1016. https://doi.org/10.1016/j.energy.2012.04.048

Lei, Z., Dai, C., Chen, B., 2014. Gas solubility in ionic liquids. Chem. Rev. https://doi.org/10.1021/cr300497a

Linstrom, P.J., Mallard, W.G., 2014. NIST Chemistry webBook, NIST Standard Reference Database Number 69, National Institute of Standards and Technology. https://doi.org/citeulike-article-id:3211271

Liu, X., He, M., Lv, N., Qi, X., Su, C., 2015a. Solubilities of R-161 and R-143a in 1-Hexyl-3-methylimidazolium bis(trifluoromethylsulfonyl)imide. Fluid Phase Equilib. 388, 37–42. https://doi.org/10.1016/j.fluid.2014.12.026

Liu, X., He, M., Lv, N., Qi, X., Su, C., 2015b. Vapor-liquid equilibrium of three hydrofluorocarbons with [HMIM][Tf2N]. J. Chem. Eng. Data 60, 1354–1361. https://doi.org/10.1021/je501069b

Liu, X., Pan, P., He, M., 2018. Vapor-liquid equilibrium and diffusion coefficients of R32 + [HMIM][FEP], R152a + [HMIM][FEP] and R161 + [HMIM][FEP]. J. Mol. Liq. 253, 28–35. https://doi.org/10.1016/j.molliq.2018.01.032

Liu, X., Qi, X., Lv, N., He, M., 2015c. Gaseous absorption of fluorinated ethanes by ionic liquids. Fluid Phase Equilib. 405, 1–6. https://doi.org/10.1016/j.fluid.2015.07.001

Llovell, F., Marcos, R.M., Vega, L.F., 2013. Transport properties of mixtures by the soft-

SAFT + Free-volume theory: Application to mixtures of n-alkanes and hydrofluorocarbons. J. Phys. Chem. B 117. https://doi.org/10.1021/jp401754r

Llovell, F., Oliveira, M.B., Coutinho, J.A.P., Vega, L.F., 2015. Solubility of greenhouse and acid gases on the [C_4mim][$MeSO_4$] ionic liquid for gas separation and CO_2 conversion. Catal. Today 255, 87–96. https://doi.org/10.1016/j.cattod.2014.12.049

Llovell, F., Pàmies, J.C., Vega, L.F., 2004. Thermodynamic properties of Lennard-Jones chain molecules: Renormalization-group corrections to a modified statistical associating fluid theory. J. Chem. Phys. 121, 10715–10724. https://doi.org/10.1063/1.1809112

Llovell, F., Valente, E., Vilaseca, O., Vega, L.F., 2011. Modeling complex associating mixtures with [$C_n$mim][Tf_2N] ionic liquids: Predictions from the soft-SAFT equation. J. Phys. Chem. B 115, 4387–4398. https://doi.org/10.1021/jp112315b

Llovell, F., Vilaseca, O., Vega, L.F., 2012. Thermodynamic Modeling of Imidazolium-Based Ionic Liquids with the [PF_6]− Anion for Separation Purposes. Sep. Sci. Technol. 47, 399–410. https://doi.org/10.1080/01496395.2011.635625

Meindersma, G.W., Podt, A.J.G., de Haan, A.B., 2006. Ternary liquid-liquid equilibria for mixtures of toluene + n-heptane + an ionic liquid. Fluid Phase Equilib. 247, 158–168. https://doi.org/10.1016/j.fluid.2006.07.002

Mota-Babiloni, A., Makhnatch, P., Khodabandeh, R., 2017. Recent investigations in HFCs substitution with lower GWP synthetic alternatives: Focus on energetic performance and environmental impact. Int. J. Refrig. 82, 288–301. https://doi.org/10.1016/j.ijrefrig.2017.06.026

Mota-Babiloni, A., Navarro-Esbrí, J., Barragán-Cervera, Á., Molés, F., Peris, B., 2015. Analysis based on EU Regulation No 517/2014 of new HFC/HFO mixtures as alternatives of high GWP refrigerants in refrigeration and HVAC systems. Int. J. Refrig. 52, 21–31. https://doi.org/10.1016/j.ijrefrig.2014.12.021

Mota-Martinez, M.T., Brandl, P., Hallett, J.P., Mac Dowell, N., 2018. Challenges and opportunities for the utilisation of ionic liquids as solvents for CO2 capture. Mol. Syst. Des. Eng. 3, 560–571. https://doi.org/10.1039/c8me00009c

Noda, A., Hayamizu, K., Watanabe, M., 2001. Pulsed-gradient spin-echo 1H and 19F NMR

ionic diffusion coefficient, viscosity, and ionic conductivity of non-chloroaluminate room-temperature ionic liquids. J. Phys. Chem. B 105, 4603–4610. https://doi.org/10.1021/jp004132q

Noelke, C.J., Shiflett, M.B., 2013. Capture of fluorinated vinyl monomers using ionic liquids. US 2013/0296499 A1.

Oliveira, M.B., Llovell, F., Coutinho, J.A.P., Vega, L.F., 2012. Modeling the [NTf_2] pyridinium ionic liquids family and their mixtures with the soft statistical associating fluid theory equation of state. J. Phys. Chem. B 116, 9089–9100. https://doi.org/10.1021/jp303166f

Pardo, F., Zarca, G., Urtiaga, A., 2020. Separation of Refrigerant Gas Mixtures Containing R32, R134a, and R1234yf through Poly(ether- block -amide) Membranes. ACS Sustain. Chem. Eng. 8, 2548–2556. https://doi.org/10.1021/acssuschemeng.9b07195

Pereira, L.M.C., Martins, V., Kurnia, K.A., Oliveira, M.B., Dias, A.M.A., Llovell, F., Vega, L.F., Carvalho, P.J., Coutinho, J.A.P., 2016. High pressure solubility of CH_4, N_2O and N_2 in 1-butyl-3-methylimidazolium dicyanamide: Solubilities, selectivities and soft-SAFT modeling. J. Supercrit. Fluids 110, 56–64. https://doi.org/10.1016/j.supflu.2015.12.006

Pereira, L.M.C., Oliveira, M.B., Dias, A.M.A., Llovell, F., Vega, L.F., Carvalho, P.J., Coutinho, J.A.P., 2013. High pressure separation of greenhouse gases from air with 1-ethyl-3-methylimidazolium methyl-phosphonate. Int. J. Greenh. Gas Control 19, 299–309. https://doi.org/10.1016/j.ijggc.2013.09.007

Pereira, L.M.C., Oliveira, M.B., Llovell, F., Vega, L.F., Coutinho, J.A.P., 2014. Assessing the N_2O/CO_2 high pressure separation using ionic liquids with the soft-SAFT EoS. J. Supercrit. Fluids 92, 231–241. https://doi.org/10.1016/j.supflu.2014.06.005

Ren, W., Scurto, A.M., 2009. Phase equilibria of imidazolium ionic liquids and the refrigerant gas, 1,1,1,2-tetrafluoroethane (R-134a). Fluid Phase Equilib. 286, 1–7. https://doi.org/10.1016/j.fluid.2009.07.007

Schulz, M., Kourkoulas, D., 2014. Regulation (EU) No 517/2014 of the European Parliament and of the Council of 16 April 2014 on fluorinated greenhouse gases and repealing Regulation (EC) No 842/2006. Off. J. Eur. Union 2014, L150/195-230.

https://doi.org/https://doi.org/10.4271/1999-01-0874

Shariati, A., Ashrafmansouri, S.S., Osbuei, M.H., Hooshdaran, B., 2013. Critical properties and acentric factors of ionic liquids. Korean J. Chem. Eng. 30, 187–193. https://doi.org/10.1007/s11814-012-0118-9

Shariati, A., Gutkowski, K., Peters, C.J., 2005. Comparison of the phase behavior of some selected binary systems with ionic liquids. AIChE J. 51, 1532–1540. https://doi.org/10.1002/aic.10384

Shiflett, M.B., 2015. Capture of trifluoromethane using ionic liquids. US 2015/082981 A1.

Shiflett, M.B., Harmer, M.A., Junk, C.P., Yokozeki, A., 2006a. Solubility and diffusivity of 1,1,1,2-tetrafluoroethane in room-temperature ionic liquids. Fluid Phase Equilib. 242, 220–232. https://doi.org/10.1016/j.fluid.2006.01.026

Shiflett, M.B., Harmer, M.A., Junk, C.P., Yokozeki, A., 2006b. Solubility and diffusivity of difluoromethane in room-temperature ionic liquids. J. Chem. Eng. Data 51, 483–495. https://doi.org/10.1021/je050386z

Shiflett, M.B., Shiflett, A.D., Yokozeki, A., 2011. Separation of tetrafluoroethylene and carbon dioxide using ionic liquids. Sep. Purif. Technol. 79, 357–364. https://doi.org/10.1016/j.seppur.2011.03.023

Shiflett, M.B., Yokozeki, A., 2014a. Process for purifying perfluorinated products. US 8,771,626 B2.

Shiflett, M.B., Yokozeki, A., 2014b. Utilizing ionic liquids for hydrofluorocarbon separation. US 8,628,644 B2.

Shiflett, M.B., Yokozeki, A., 2012. Process for separation of tetrafluoroethylene from carbon dioxide using ionic liquids. US 8,313,558 B2.

Shiflett, M.B., Yokozeki, A., 2011. Process for the separation of diastereomers. US 8,075,777 B2.

Shiflett, M.B., Yokozeki, A., 2010. Separation of carbon dioxide and sulfur dioxide using room-temperature ionic liquid [bmim][MeSO4]. Energy and Fuels 24, 1001–1008. https://doi.org/10.1021/ef900997b

Shiflett, M.B., Yokozeki, A., 2009. Solubility of Fluorocarbons in Room Temperature Ionic

Liquids, in: Ionic Liquids: From Knowledge to Application. ACS, pp. 21–42. https://doi.org/10.1021/bk-2009-1030

Shiflett, M.B., Yokozeki, A., 2008. Binary vapor-liquid and vapor-liquid-liquid equilibria of hydrofluorocarbons (HFC-125 and HFC-143a) and hydrofluoroethers (HFE-125 and HFE-143a) with ionic liquid [emim][Tf2N]. J. Chem. Eng. Data 53, 492–497. https://doi.org/10.1021/je700588d

Shiflett, M.B., Yokozeki, A., 2007. Solubility differences of halocarbon isomers in ionic liquid [emim][Tf2N]. J. Chem. Eng. Data 52, 2007–2015. https://doi.org/10.1021/je700295e

Shiflett, M.B., Yokozeki, A., 2006a. Vapor-liquid-liquid equilibria of pentafluoroethane and ionic liquid [bmim][PF6] mixtures studied with the volumetric method. J. Phys. Chem. B 110, 14436–14443. https://doi.org/10.1021/jp062437k

Shiflett, M.B., Yokozeki, A., 2006b. Vapor - Liquid - Liquid equilibria of hydrofluorocarbons + 1-butyl-3-methylimidazolium hexafluorophosphate. J. Chem. Eng. Data 51, 1931–1939. https://doi.org/10.1021/je060275f

Shiflett, M.B., Yokozeki, A., 2006c. Gaseous absorption of fluoromethane, fluoroethane, and 1,1,2,2-tetrafluoroethane in 1-butyl-3-methylimidazolium hexafluorophosphate. Ind. Eng. Chem. Res. 45, 6375–6382. https://doi.org/10.1021/ie060192s

Shiflett, M.B., Yokozeki, A., 2006d. Separation of difluoromethane and pentafluoroethane by extractive distillation using ionic liquid. Chim. Oggi 24, 28–30.

Shiflett, M.B., Yokozeki, A., 2006e. Solubility and diffusivity of hydrofluorocarbons in room-temperature ionic liquids. AIChE J. 52, 1205–1219. https://doi.org/10.1002/aic.10685

Shiflett, Yokozeki, A., Knapp, J.P., 2011. Process for the separation of fluorocarbons using ionic liquids. US 7,964,760 B2.

Sujatha, I., Venkatarathnam, G., 2018. Comparison of performance of a vapor absorption refrigeration system operating with some hydrofluorocarbons and hydrofluoroolefins as refrigerants along with ionic liquid [hmim][TF2N] as the absorbent. Int. J. Refrig. 88, 370–382.

https://doi.org/10.1016/j.ijrefrig.2018.03.004

Urahata, S.M., Ribeiro, M.C.C., 2004. Structure of ionic liquids of 1-alkyl-3-methylimidazolium cations: A systematic computer simulation study. J. Chem. Phys. 120, 1855–1863. https://doi.org/10.1063/1.1635356

Vatani, M., Asghari, M., Vakili-Nezhaad, G., 2012. Application of Genetic Algorithm to the calculation of parameters for NRTL and Two-Suffix Margules models in ternary extraction ionic liquid systems. J. Ind. Eng. Chem. 18, 1715–1720. https://doi.org/10.1016/j.jiec.2012.03.008

Vega, L.F., Vilaseca, O., Llovell, F., Andreu, J.S., 2010. Modeling ionic liquids and the solubility of gases in them: Recent advances and perspectives. Fluid Phase Equilib. 294, 15–30. https://doi.org/10.1016/j.fluid.2010.02.006

Vilaseca, O., Llovell, F., Yustos, J., Marcos, R.M., Vega, L.F., 2010. Phase equilibria, surface tensions and heat capacities of hydrofluorocarbons and their mixtures including the critical region. J. Supercrit. Fluids 55, 755–768. https://doi.org/10.1016/j.supflu.2010.10.015

Wasserscheid, P., Van Hal, R., Bösmann, A., 2002. 1-n-butyl-3-methylimidazolium ([bmim]) octylsulfate - An even "greener" ionic liquid. Green Chem. 4, 400–404. https://doi.org/10.1039/b205425f

Yokozeki, A., Shiflett, M.B., 2009. Separation of carbon dioxide and sulfur dioxide gases using room-temperature ionic liquid [hmim][Tf2N]. Energy and Fuels 23, 4701–4708. https://doi.org/10.1021/ef900649c

Yokozeki, A., Shiflett, M.B., 2007. Vapor-liquid equilibria of ammonia + ionic liquid mixtures. Appl. Energy 84, 1258–1273. https://doi.org/10.1016/j.apenergy.2007.02.005

Yokozeki, A., Shiflett, M.B., 2006. Global phase behaviors of trifluoromethane in ionic liquid [bmim][PF 6]. AIChE J. 52, 3952–3957. https://doi.org/10.1002/aic.11007

Zarca, G., Ortiz, I., Urtiaga, A., 2018. Novel solvents based on thiocyanate ionic liquids doped with copper(I) with enhanced equilibrium selectivity for carbon monoxide separation from light gases. Sep. Purif. Technol. 196, 47–56. https://doi.org/10.1016/j.seppur.2017.06.069

Zarca, G., Ortiz, I., Urtiaga, A., Llovell, F., 2017a. Accurate thermodynamic modeling of ionic liquids/metal salt mixtures: Application to carbon monoxide reactive absorption. AIChE J. 63, 3532–3543. https://doi.org/10.1002/aic.15790

Zarca, G., Ortiz, I., Urtiaga, A., Llovell, F., 2017b. Modelling the physical properties of ionic liquid/metal salt mixtures with the soft-SAFT equation of state: application to carbon monoxide reactive separation. Comput. Aided Chem. Eng. 40, 217–222. https://doi.org/10.1016/B978-0-444-63965-3.50038-6

Zhao, Y., Gani, R., Afzal, R.M., Zhang, X., Zhang, S., 2017. Ionic liquids for absorption and separation of gases: An extensive database and a systematic screening method. AIChE J. 63, 1353–1367. https://doi.org/10.1002/aic.15618

List of Tables

Table 1. *Main properties of the refrigerant gases studied in this work (Honeywell Genetron Properties Suite, 2016).*

Property	**R32**	**R125**	**R410A**
Molecular formula	CH_2F_2	C_2HF_5	CH_2F_2 + C_2HF_5 (69.8/30.2 mol%)
Molecular weight (g mol^{-1})	52.024	120.02	72.585
Normal boiling point (K)	221.50	225.06	~221.75
Critical temperature (K)	351.26	339.17	344.49
Critical pressure (MPa)	5.7820	3.6177	4.9013
GWP (CO_2-eq., 100 yr)*	677	3170	2088

**Values taken from the IPCC fifth assessment report (IPCC — Intergovernmental Panel on Climate Change, 2015)*

Table 2. *Soft-SAFT molecular parameters of the HFCs and ILs investigated in this work.*

Compound	m	σ (Å)	ε/k_B (K)	ε^{HB}/k_B (K)	κ^{HB} (Å^3)	**Range (K)**	**Reference**
HFC-R32	1.321	3.529	144.4	1708	24050	180-333	This work
HFC-R125	1.392	4.242	148.8	1685	24050	180-333	This work
[C_2mim][Tf_2N]	6.023	4.069	394.6	3450	2250	-	(Llovell et al., 2011)
[C_6mim][Tf_2N]	6.338	4.334	404.2	3450	2250	-	(Llovell et al., 2011)
[C_4mim][PF_6]	4.570	4.146	418.0	3450	2250	-	(Andreu and Vega, 2007)

Table 3. *Binary energy and size parameters for the studied HFCs + ionic liquid systems*.

Ionic liquid	HFC	ξ	η
$[C_2mim][Tf_2N]$	R32	1.185	1.052
	R125	1.236	1.052
$[C_6mim][Tf_2N]$	R32	1.180	1.052
	R125	1.230	1.052
$[C_4mim][PF_6]$	R32	1.238	1.052
	R125	1.266	1.070

Table 4. *Enthalpy and entropy of solvation of R32 and R125 in selected ILs.*

Ionic liquid	HFC	ΔH (kJ mol^{-1})	ΔS (J mol^{-1} K^{-1})
$[C_2mim][Tf_2N]$	R32	-21.5	-68.3
	R125	-20.1	-63.8
$[C_6mim][Tf_2N]$	R32	-20.5	-63.5
	R125	-19.0	-59.0
$[C_4mim][PF_6]$	R32	-18.8	-59.6
	R125	-16.0	-50.7

Table 5. *ASPEN Plus simulation for the separation of R410A*

Feed	
Flow rate (kg s^{-1})	0.3000
R32 flow rate (kg s^{-1})	0.1500
R125 flow rate (kg s^{-1})	0.1500
R410A inlet temperature (K)	303.15
[C_2mim][Tf_2N] flow rate (kg s^{-1})	4.2464
[C_2mim][Tf_2N] inlet temperature (K)	313.15
Main Column	
Condenser temperature (K)	286.3
Condenser heat duty (kW)	-29.11
Distillate rate (kg s^{-1})	0.1218
R125 overhead mole fraction	0.9900
Reboiler temperature (K)	353.7
Reboiler heat duty (kW)	1955
Bottoms rate (kg s^{-1})	4.425
Operating pressure (MPa)	1.000
Theoretical stages	28.00
R410A feed stage	22.00
[C_2mim][Tf_2N] feed stage	2.000
Flash Drum 1	
Outlet Pressure (MPa)	0.1000
Outlet temperature (K)	353.7
R32 overhead flow rate (kg s^{-1})	0.1354
R32 overhead mole fraction	0.9196
Flash Drum 2	
Outlet Pressure (MPa)	0.0100
Outlet temperature (K)	353.73
R32 overhead flow rate (kg s^{-1})	0.0139
R32 overhead mole fraction	0.9569
Cooler	
Heat duty (kW)	1957
Pump	
Net Work Required (kW)	6.834

List of Figures

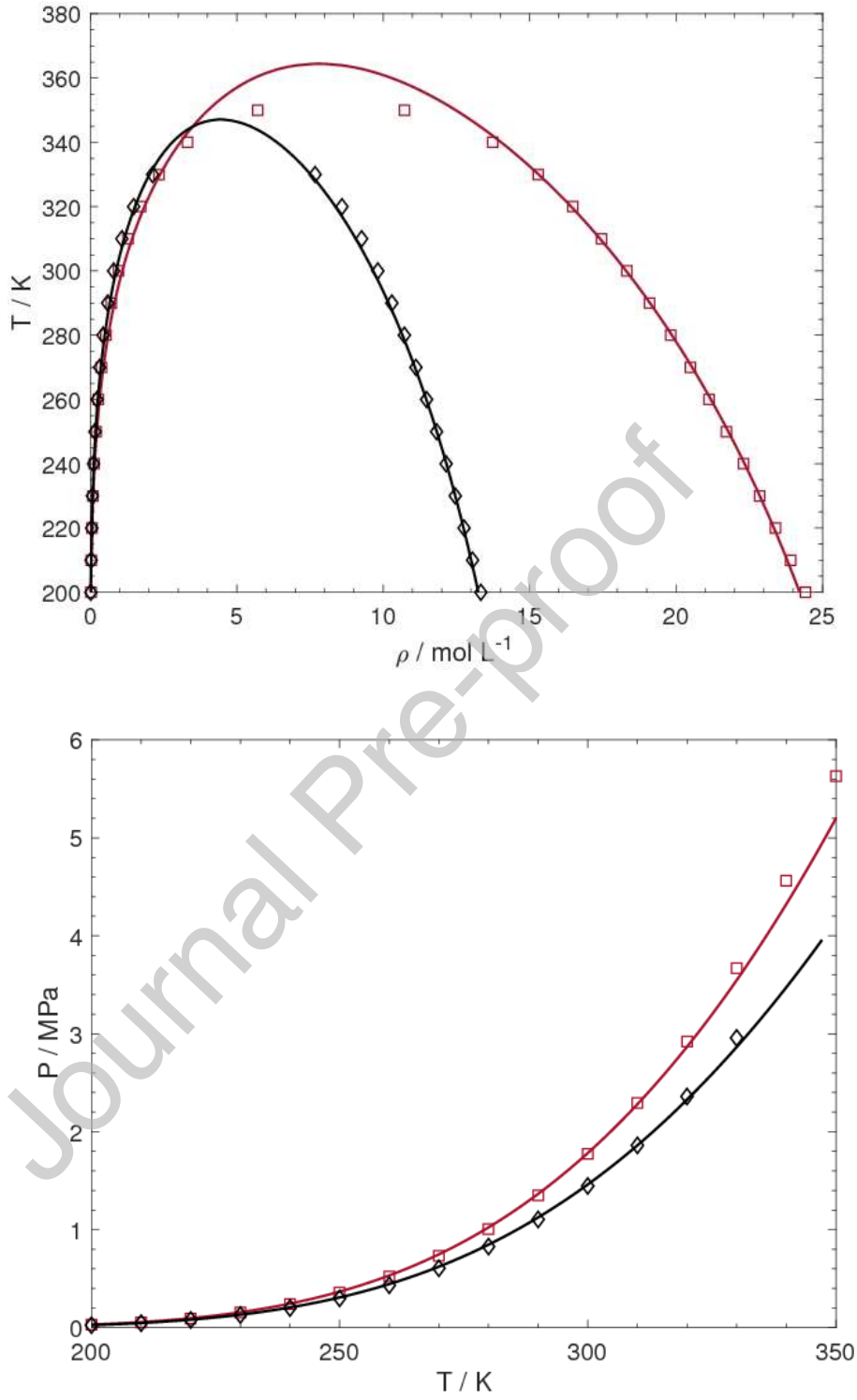

Figure 1. *Phase equilibria of R32 (red squares) and R125 (black diamonds). (a) Coexisting vapor and liquid densities and (b) vapor pressure vs. temperature. Symbols represent the correlated data from experimental measurements (Linstrom and Mallard, 2014) and solid lines are the soft-SAFT calculations.*

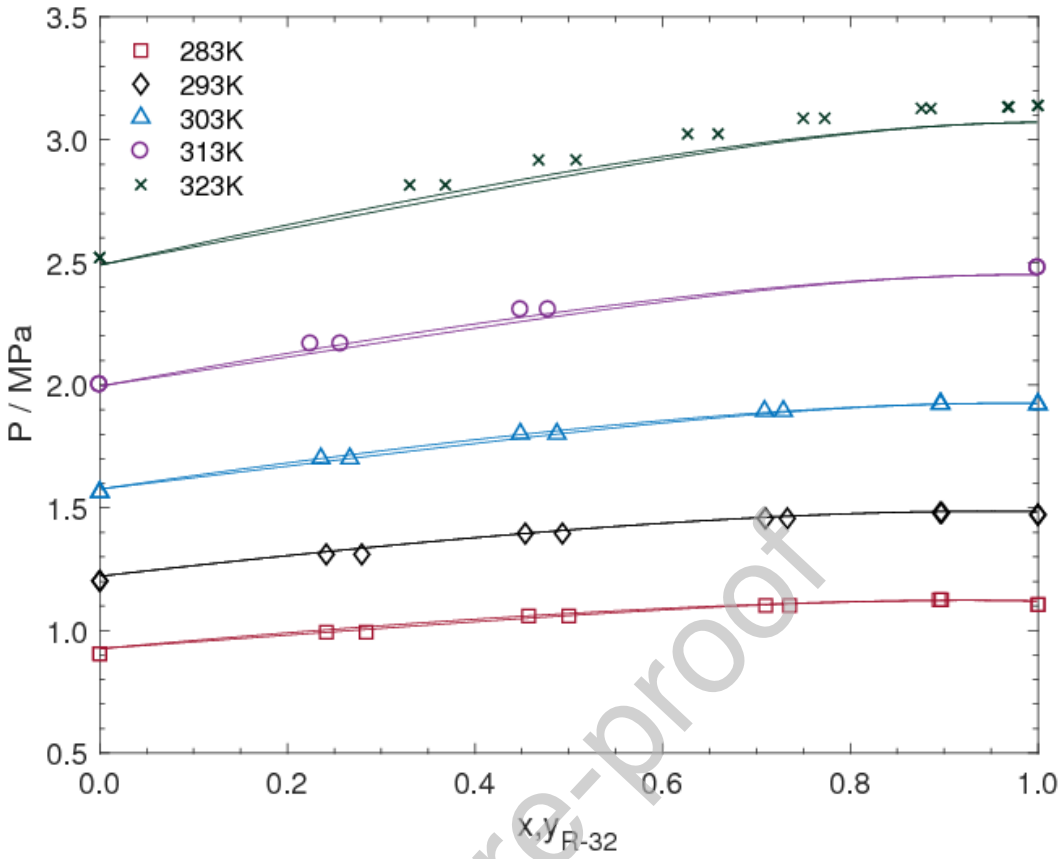

***Figure 2**. Vapor-liquid equilibria for the system R32 + R125 at 283.15 (red squares), 293.15 (black diamonds), 303.15 (blue triangles), 313.15 (violet circles) and 323.15 K (green crosses). Symbols represent the experimental data* (Higashi, 1997) *and solid lines are the soft-SAFT calculations obtained in the present study*.

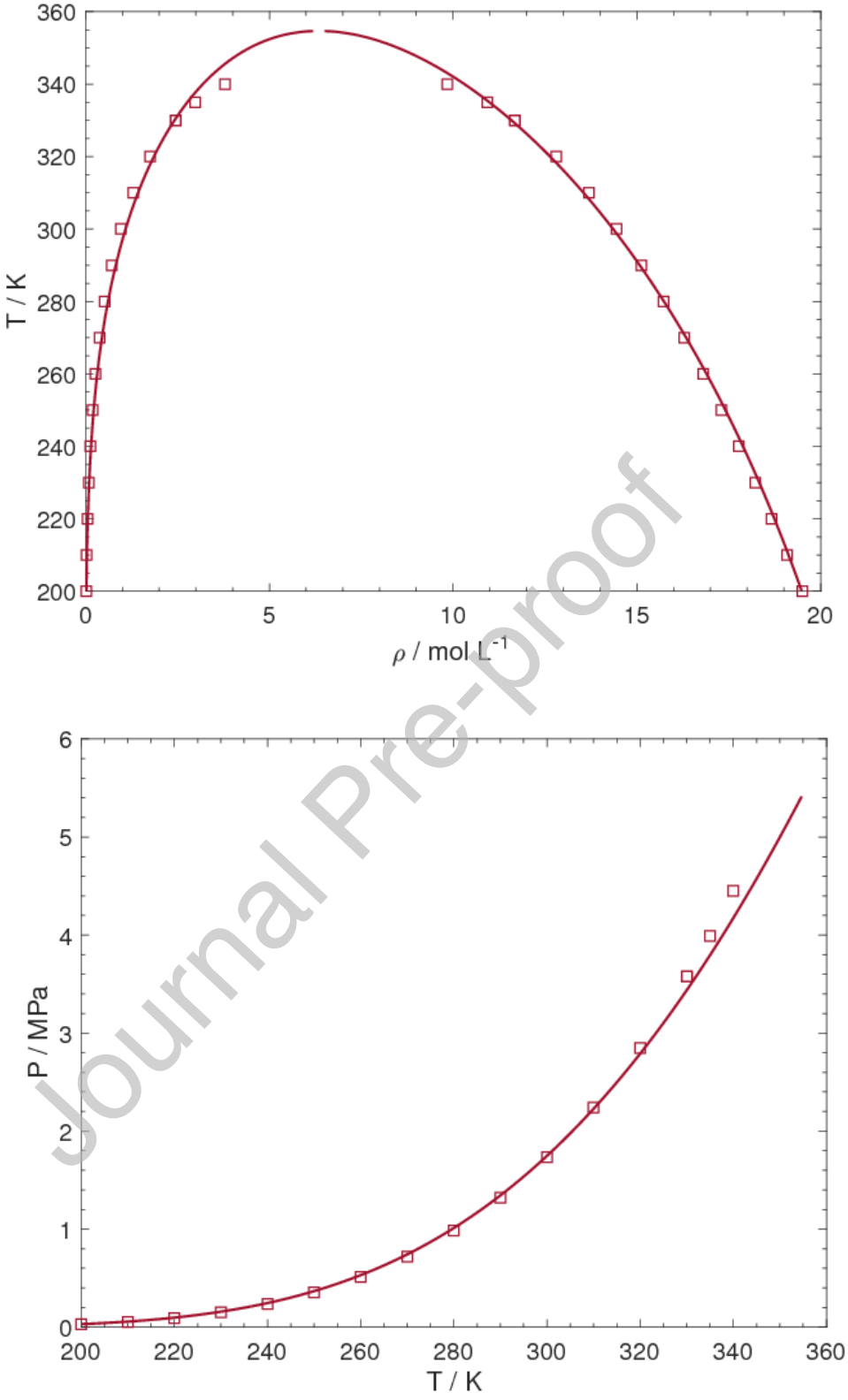

Figure 3. *Predicted vapor-liquid equilibria of blend R410A. a) Temperature-density, and b) pressure-temperature diagrams. Symbols represent correlated data from experimental measurements (Honeywell Genetron Properties Suite, 2016) and solid lines are the soft-SAFT calculations.*

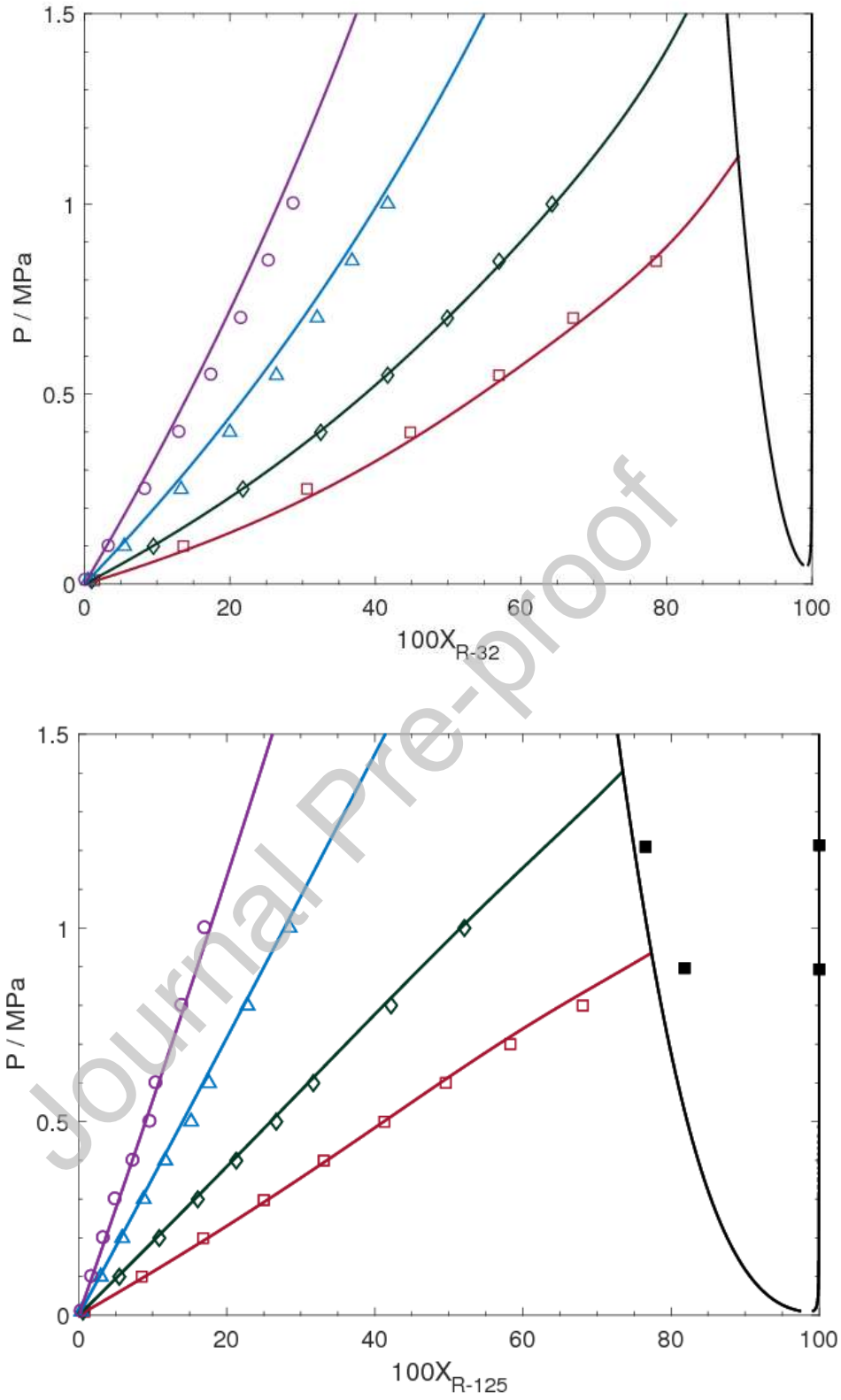

Figure 4. *Pressure-composition diagram of (a) R32 + [C_2mim][Tf_2N] and (b) R125 + [C_2mim][Tf_2N] at several temperatures: 283.15 (red squares), 298.15 (green diamonds), 323.15 (blue triangles) and 348.15 K (violet circles). Symbols represent the experimental data* (Shiflett et al., 2006b; Shiflett and Yokozeki, 2008) *and solid lines are the soft-SAFT calculations. The black curve represents the prediction of the VLL three-phase line.*

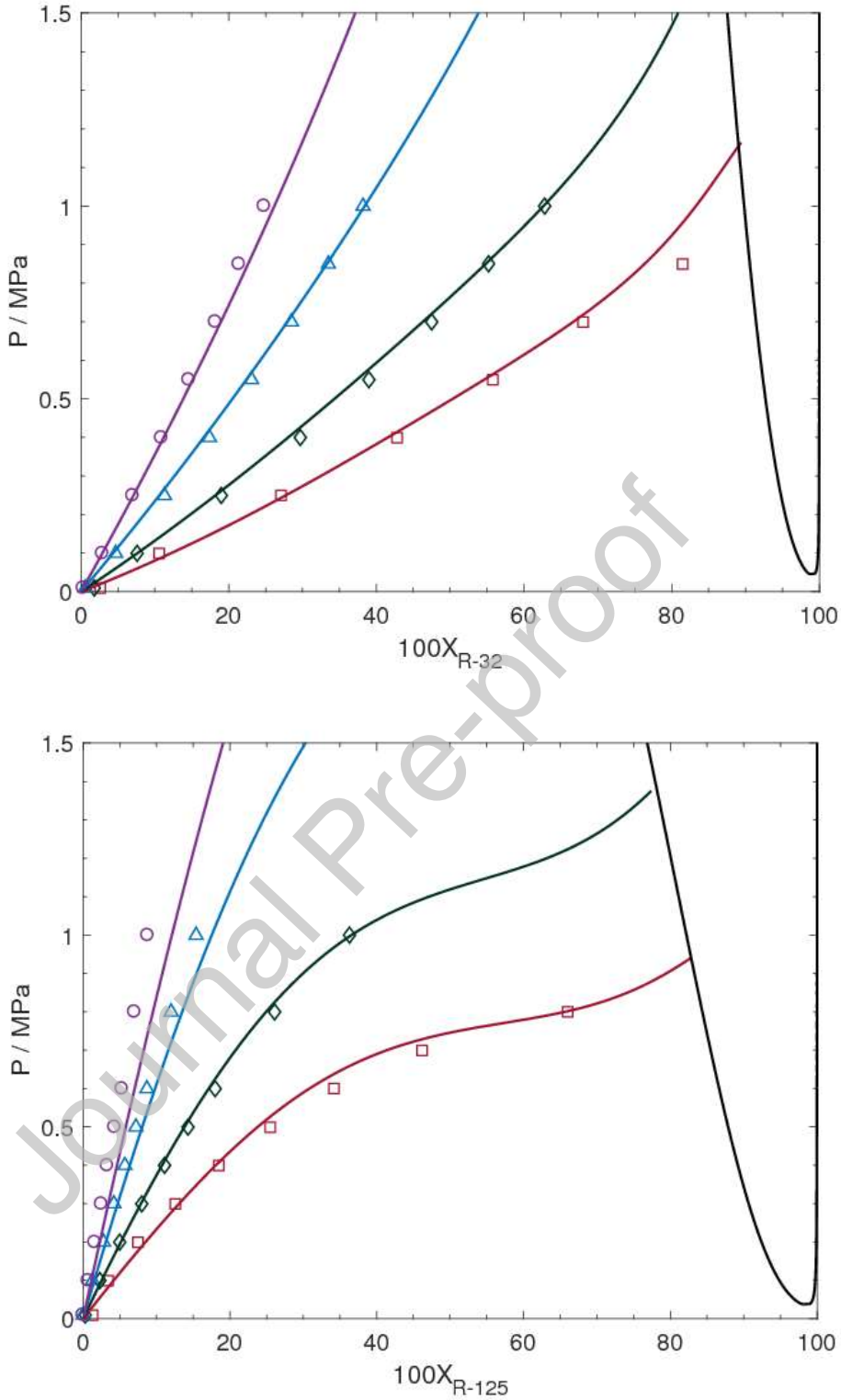

Figure 5. *Pressure-composition diagram of the G-L systems (a) R32 + [C_4mim][PF_6] and (b) R125 + [C_4mim][PF_6] at several temperatures: 283.15 (red squares), 298.15 (green diamonds), 323.15 (blue triangles) and 348.15 K (violet circles). Symbols represent the experimental data (Yokozeki and Shiflett, 2006) and solid lines are the soft-SAFT calculations. The black curve represents the prediction of the Vapor-liquid-liquid three-phase line.*

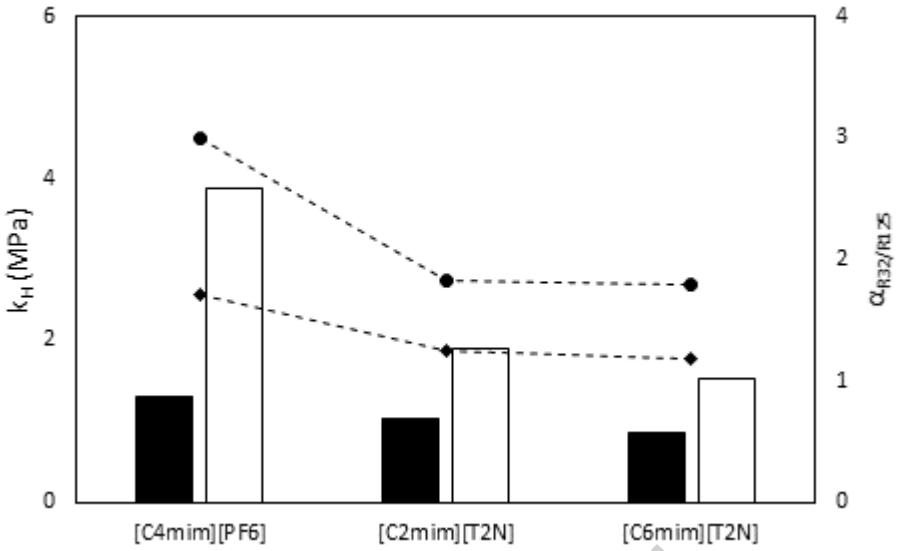

Figure 6. *Calculated Henry's law constants for R32 (black) and R125 (white) and ideal selectivity at infinite dilution (circles) and 1.0 MPa (diamonds) in [C_4mim][PF_6] and [C_2mim][Tf_2N] at 298.15 K and [C_6mim][Tf_2N] at 303.15 K.*

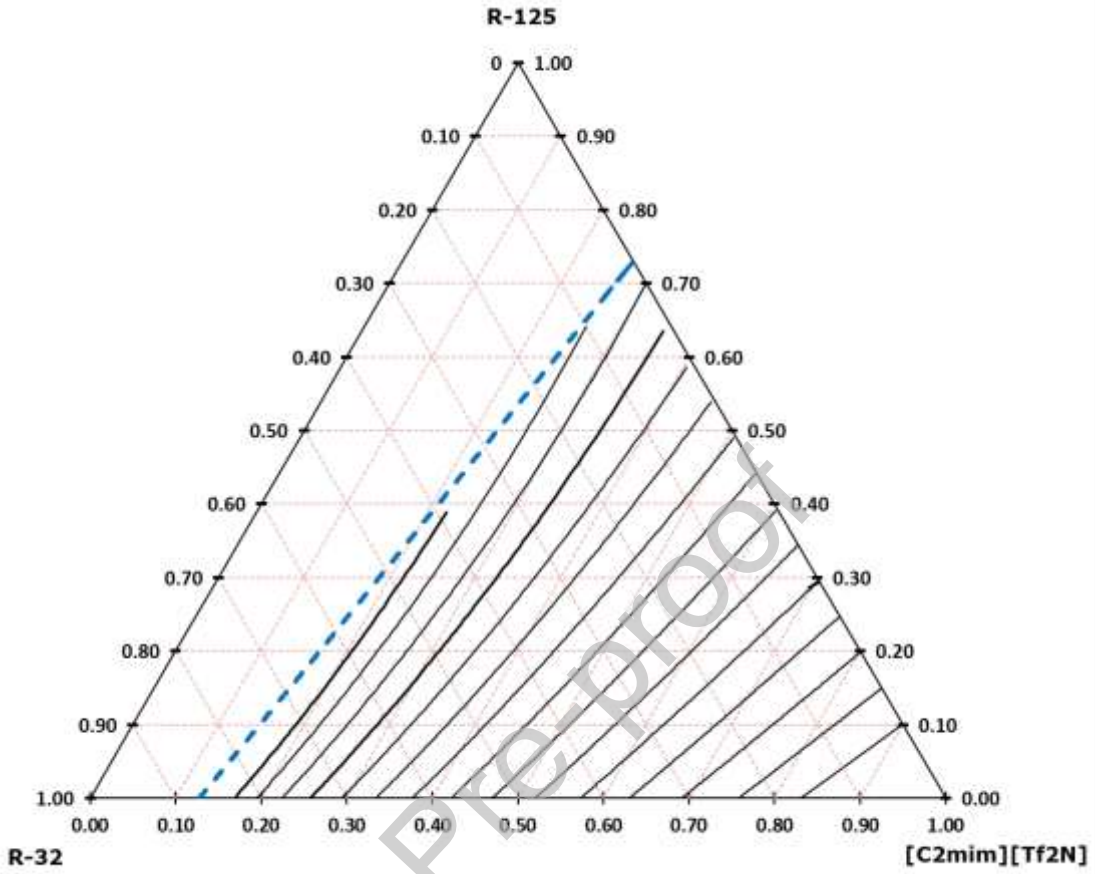

Figure 7. *Isothermal ternary phase diagram predicted with soft-SAFT for the system R32 + R125 + [C_2mim][Tf_2N] at 300 K. The different curves represent predicted isobars at pressures ranging from 0.2 (bottom line) to 1.6 MPa (upper line) at 0.1 MPa intervals. The dashed blue line corresponds to the VLLE curve.*

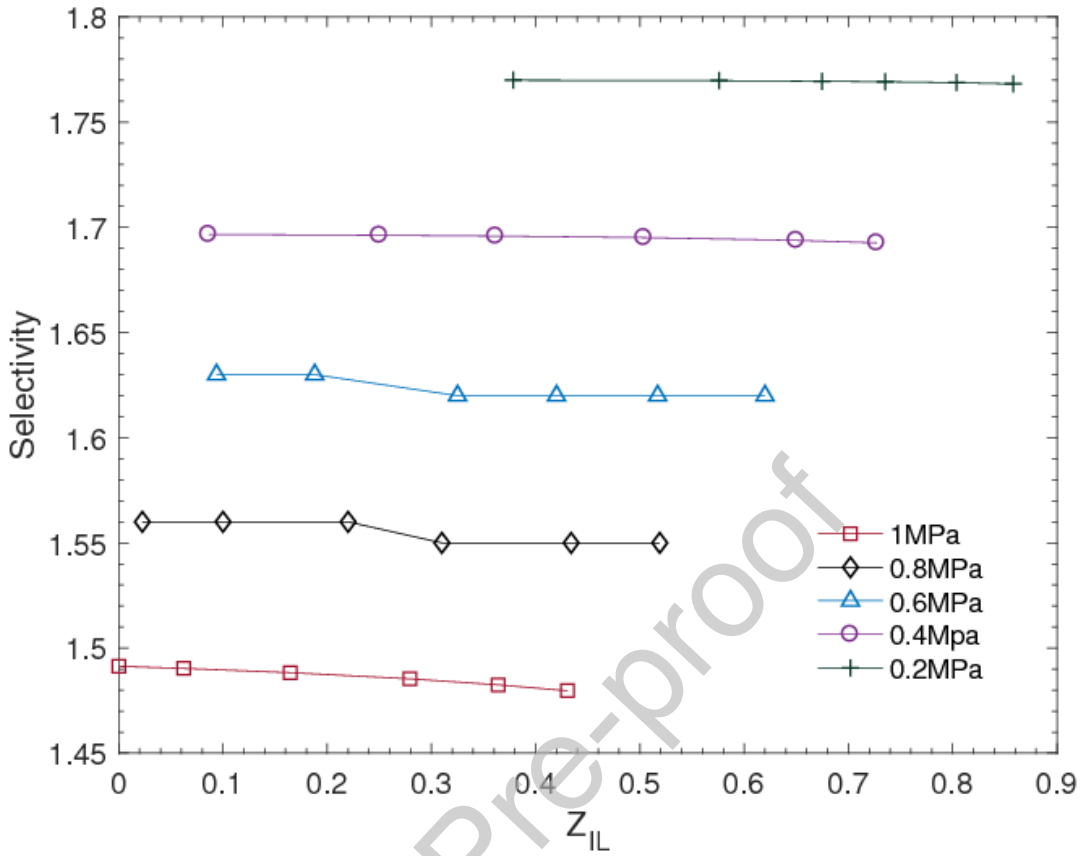

***Figure 8**. Predicted separation performance (Selectivity calculated as Eq (7)) for the recovery of R32 from R410A as a function of the [C_2mim][Tf_2N] feed mole fraction (Z_{IL}) at 300 K and several pressures: 0.2 (green crosses), 0.4 (violet circles), 0.6 (blue triangles), 0.8 (black diamonds) and 1 MPa (red squares).*

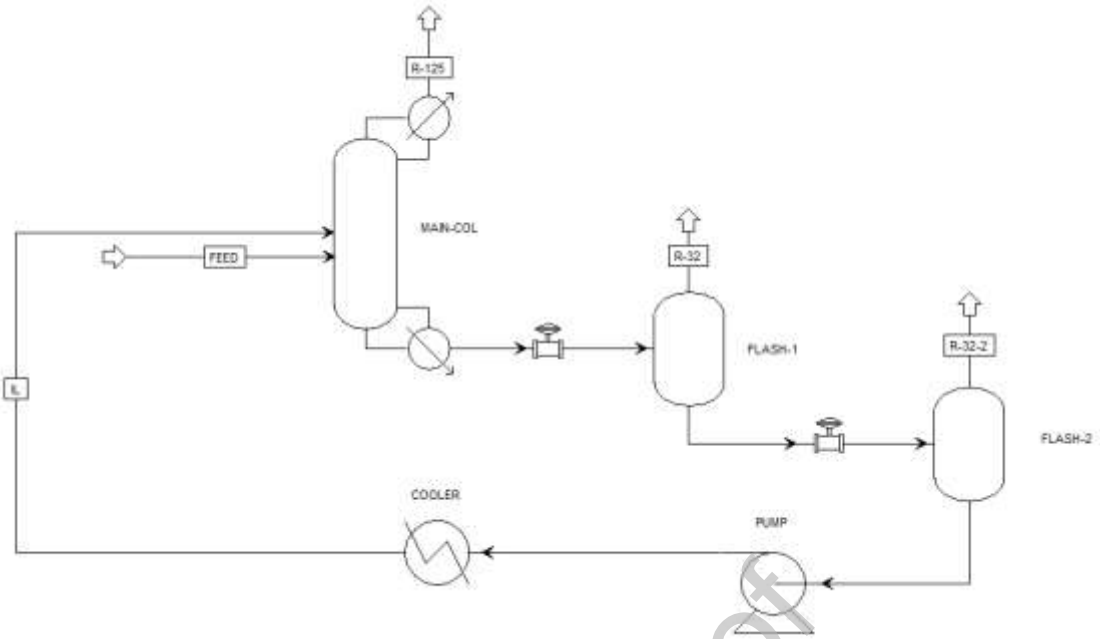

Figure 9. *Main process flowsheet of a separation unit of the R410 blend using [C_2mim][Tf_2N] as entrainer. The diagram contains a distillation column (MAIN-COL) for the removal of R125 followed by two flash tanks (FLASH-1 and FLASH-2) for the regeneration of the IL and removal of R32. The IL recirculation line includes a pump with a heat exchanger to cool the IL before returning to the main column.*

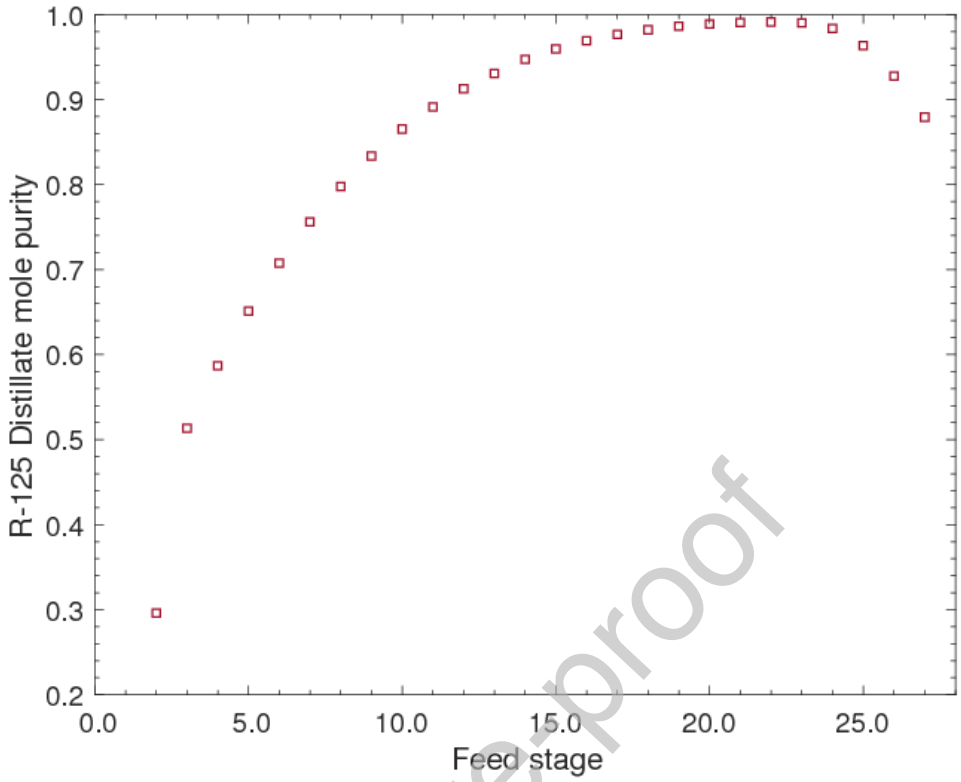

Figure 10. *Influence of the feed stage on the distillate (R125) mole purity.*

Declaration of interests

x The authors declare that they have no known competing financial interests or personal relationships that could have appeared to influence the work reported in this paper.

☐The authors declare the following financial interests/personal relationships which may be considered as potential competing interests:

Graphical Abstract